J. Fluid Mech. (1996), vol. 327, pp. 73–99

Comparative early development of wake vortices behind a short semicircular-section cylinder in two opposite arrangements

By NATHALIE BOISAUBERT, MADELEINE COUTANCEAU AND PATRICK EHRMANN

LMF/LEA, Université de Poitiers, 40, avenue du Recteur Pineau, 86022 Poitiers, France

(Received 20 April 1995 and in revised form 15 May 1996)

As a first step in a more general study of the influence of the body shape upon the initial time-development of wake vortices, we consider the case of a 5.20 aspect-ratio semicircular-section cylinder, fitted with two endplates, and with the rounded side and the flat side in turn facing the oncoming current. The flow structure is analysed by means of a detailed qualitative and quantitative analysis of numerous flow visualization pictures, for Reynolds numbers Re ranging between 60 and 600. Beyond the first phase of development, necessary for the vortex-shedding process to take place ($t^* \geqslant 6$), a change in the flow evolution with Re is found for both body configurations, at a critical Reynolds number Re_c whose final value is, within about 5%, 190 and 140 for the rounded and flat forebody respectively. However, this change varies with the body shape. Thus, above $Re = 200$, it is shown that the reversal of the body compared to the free stream (flat-forebody configuration) implies a clear difference in the wake development with a quasi-symmetrical shifting of the vortex cores to the rear of the recirculating zone and a complete annihilation of the process of vortex shedding, at least during the limited period of time corresponding to the present observation. The consequences of the modifications of the wake behaviour are quantitatively evaluated by considering the time- and Re-evolution of the wake geometrical parameters and of the axial velocity distribution; they are related to the body geometry.

1. Introduction

It is well known that wakes play a role of primary importance in aerodynamics and hydrodynamics and also in industrial devices, especially those including mass and heat transfer. Wake flows also constitute an important branch of fundamental fluid mechanics, being related to wall-separation and instability phenomena. Thus, reliable comparative data on the different structures of wake flows likely to be encountered in nature and technology are valuable for the theory to make progress, as well as to control and optimize the processes or to control aerodynamic stability and coefficients. It is with this goal that our LMFP group has undertaken a comparative study of the initial time-development, from an abrupt start, of wakes as functions of the body geometry, for moderate Reynolds numbers Re, lying between 60 (i.e. beyond the usual critical Reynolds number at which absolute instability sets in) up to $Re = 600$. Attention is focused on the body wall curvature, the eventual presence of singular points which fix the location of boundary separation and/or a hollow downstream face which induces recirculation even in the Stokes regime (Abed-Meraïm 1993). Thus, Ehrmann (1996) considers five basic geometries in turn: a solid semicircular-section

(*a*)

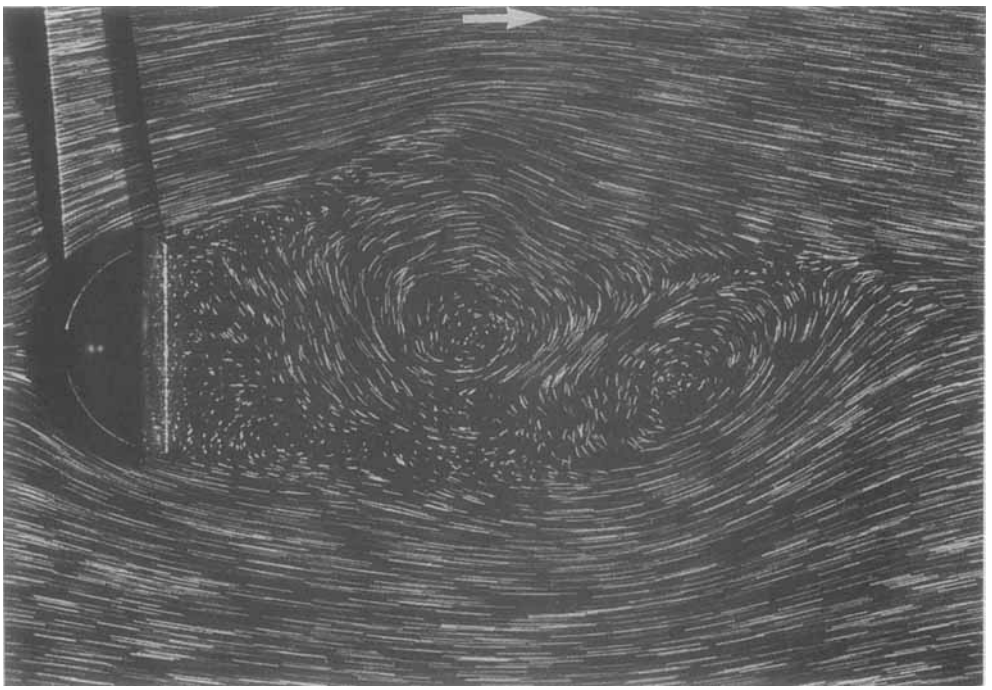

(*b*)

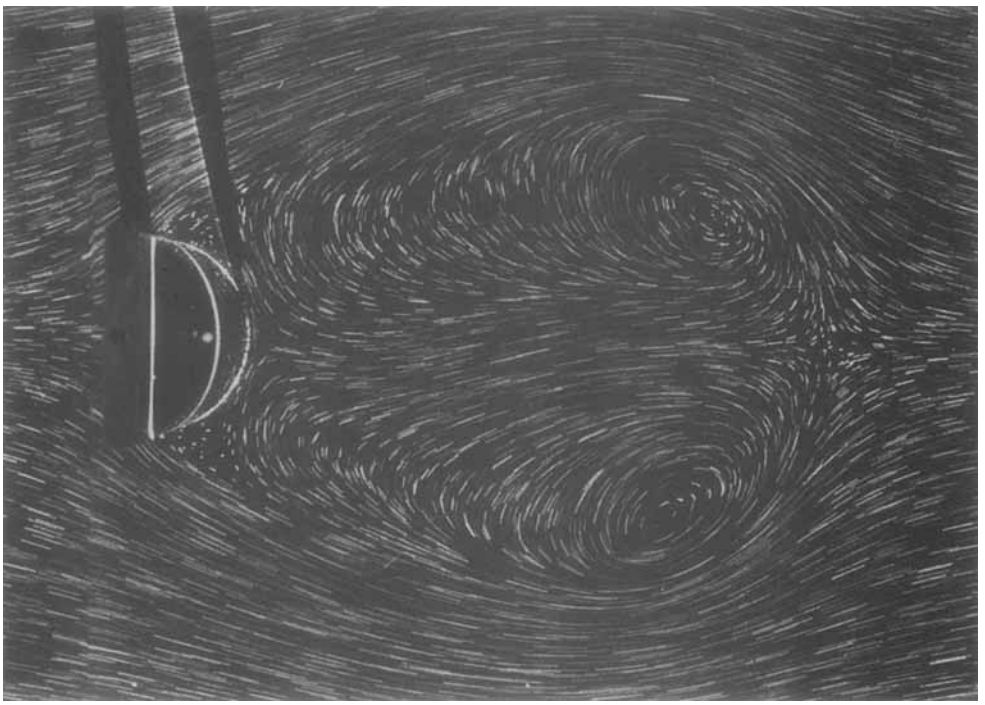

FIGURE 1. Comparative wakes of a semicircular-section cylinder for $Re = 400$, $t^* = 9$ and two opposite orientations.

cylinder in two arrangements, one where the normal flat face is turned downstream and the other upstream; a hollow semicircular shell, the cavity being at the back; a solid circular cylinder; and a normal flat plate. Both qualitative and quantitative data have been obtained for normalized time t^* up to 10. These results complete, on the one hand, those given by Coutanceau & Bouard (1977*a*, *b*), Bouard & Coutanceau (1980), and Coutanceau, Boyce & Guérineau (1988) for the circular cylinder for Re up to 10^4 and a period of time limited to $t^* = 3.5$, and on the other hand, those given by Dennis *et al.* (1993) for a normal flat plate for Re limited to 20, and by Polidori *et al.* (1992) for a circular cylinder, semicircular cylinder and normal flat plate for $0 \leqslant t^* \leqslant 10$, but for $Re = 1000$ only. It should be noticed that, except for the last two bodies, data are extremely scarce in the literature, especially regarding the wake structure (see some partial data by Gerrard (1978) and Kalra & Uhlerr (1973) for some two- and three-dimensional bodies respectively).

The objective of the work is to study the early stage of development of the very near wake induced by the different bodies which is, according to Williamson & Prasad (1993), of primary importance, because it conditions the development of the far wake itself. This study includes the identification of the vortical structures with their geometrical parameters and the evaluation of the flow kinematics by means of the determination of significant velocity profiles. These sorts of data should render possible a precise comparison between the selected wakes.

In order to indicate the important role played by body shape on the flow development, the two photographs of figure 1 show the wake downstream of cylinders having the same semicircular section and in the same flow conditions, i.e. the same end conditions, the same Reynolds number and at the same time-stage of the evolution after the start of the motion. However, the structure of these two wakes appears to be completely different. The only cause is that, in figure 1(*a*), the flat face is turned downstream whereas, in figure 1(*b*), it faces the oncoming current. This striking example justifies in itself a detailed examination of this particular problem. It is the objective of the present part of our investigation.

2. General purpose and experimental technique

We consider the way the wake is formed downstream of a semicircular cylinder of diameter D, towed vertically with a constant speed V_0 down a tall tank, by means of a very heavy and precisely guided carrier. The cylinder axis is maintained horizontal and the tank is filled with a transparent oil of suitable viscosity. The motion of the body-frame system is induced by the combination of the gravity force and of the retarding force of a dashpot, after being abruptly released from the top of the tank by cutting off an electro-magnet. The speed is adjusted to a suitable value (i.e. that corresponding to the selected Reynolds number) by the adjustment of holes drilled in the dashpot and of complementary balance weights. The precise value of V_0 is found by means of LE-diodes regularly distributed along the tank height and a device including a co-translating photo-cell associated with an electronic counter. Figure 2 gives a schematic of the experimental set-up. The section of the tank is rectangular ($W_t \times L_t = 46 \times 56$ cm^2) and may be modified eventually by the addition of vertical plates with a view to studying the influence of the wall confinement; the height is about 150 cm.

The investigation is made by means of visualization using mainly minute solid tracers uniformly dispersed in the tank oil and lit by a thin (≈ 3 mm) sheet of intense light coming either from a powerful arc-projector or a 5 W helium–argon laser.

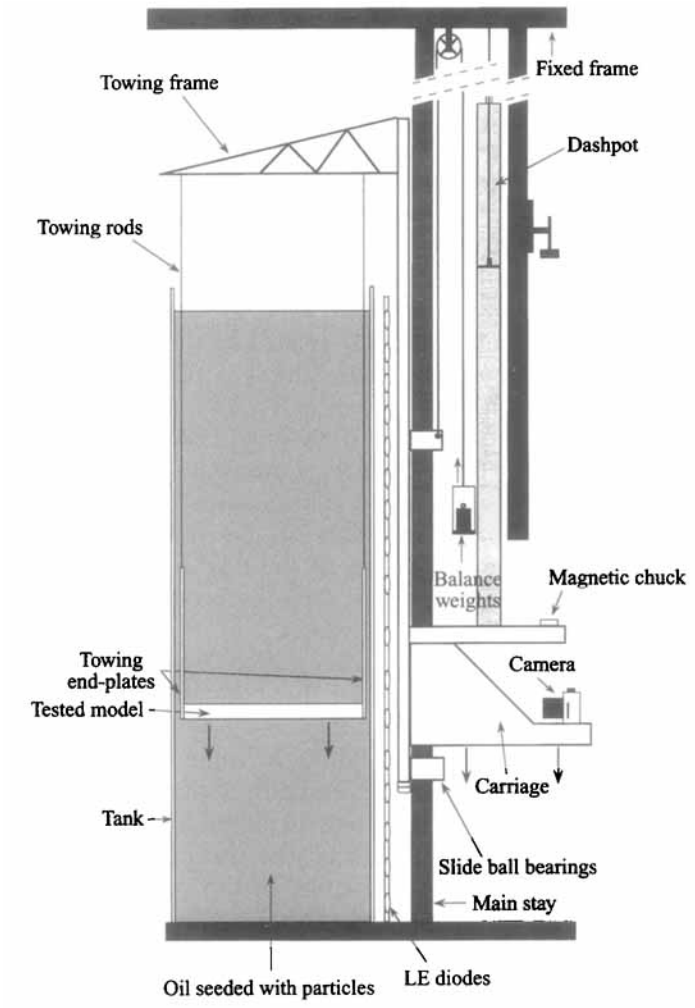

FIGURE 2. Schematic of the experimental set-up.

However, some sets of photographs have also been taken in water with an electrochemical tracer (precipitation of white hydrated tin) emitted continuously from the body wall at regularly spaced sections. In each case, the flow is sequentially recorded, with a suitable time of exposure, throughout the body downward motion by an accompanying camera (see figure 2); thus it is in a frame fixed to the body. This camera is automatically activated by means of a computer with a pre-recorded program. In this frame, the body appears to be at rest and placed in a uniform oncoming stream V_0 (figure 3).

In order to document the flow in sufficient detail, the recordings were made with a small time interval and the experiments were carried out with bodies of sufficient size ($D = 8$ cm). However, the period of normalized time t^* ($t^* = tV_0/D$) during which the flow development can be observed, as well as the aspect ratio A of the cylinder, are limited respectively by the height H_t and the width W_t of the tank, and this is more significant as the body gets bigger: $t^*_{max} < H_t/D$ and $A < W_t/D$. Also, the flow is confined by the transverse dimension L_t of the tank; let us call λ the corresponding confining ratio, i.e. D/L_t. Taking into account the selected experimental conditions,

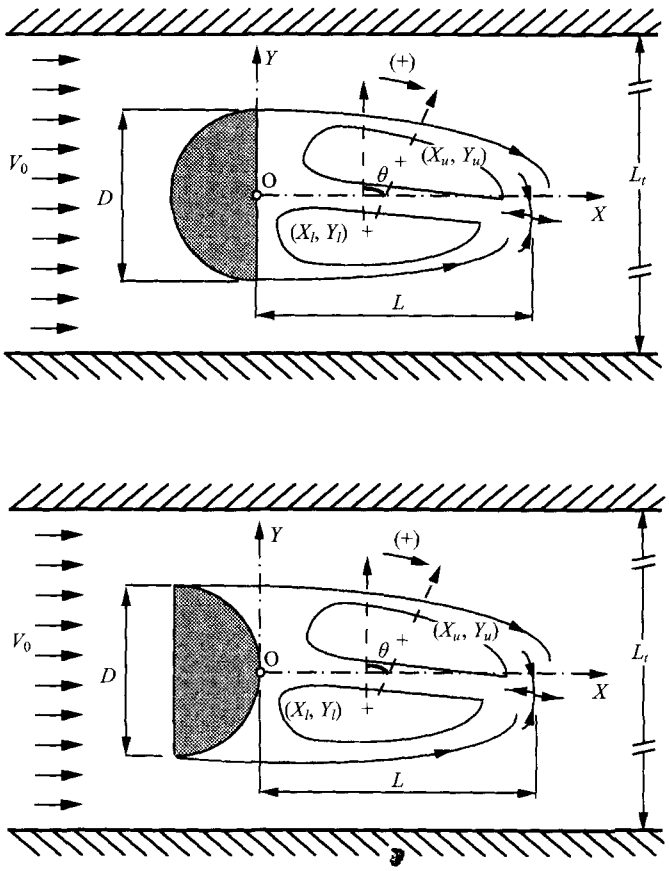

FIGURE 3. Flow schematics and parameters.

with a view to optimization the present work has been done for $A = 5.20$, $\lambda = 0.14$, $0 \leqslant t^* \leqslant 10$ in steps $\Delta t^* = 1$. The Reynolds numbers ($Re = V_0 D/\nu$) is varied between 60 and 600, in steps $\Delta Re = 100$ from $Re = 100$ onwards. In this part of the study, the pictures were taken essentially in the median cross-section.

Thus, very soon after the start of the motion, the flow appears to separate from the two sharp edges of the semicircular cylinders, inducing a recirculating zone (R-zone) which grows with time both in length and width accordingly to the following scenario, at least for the low-Re regime.

At first, this R-zone is closed and symmetrical. Then, progressively the symmetry is generally broken, one of the cores of the twin vortices is shifted downstream from the other including a stretching of the corresponding vortex and then the progressive splitting of its downstream part, whereas the upstream part retracts towards the back of the cylinder. The phenomenon becomes more marked with increasing time, provoking the complete shedding of the downstream part of the vortex and the re-organization of its upstream part into a new vortex and so progressively giving rise to an alternate vortex-shedding process by the periodic formation of a new vortex and the stretching and then the downstream splitting of the other one. It is the comparative analysis of this time-evolution that we propose to describe in the following sections, considering increasing Reynolds numbers from 60 upwards with the rounded side of the cylinder turned first upstream and then downstream, with a view to deducing the

(*a*)

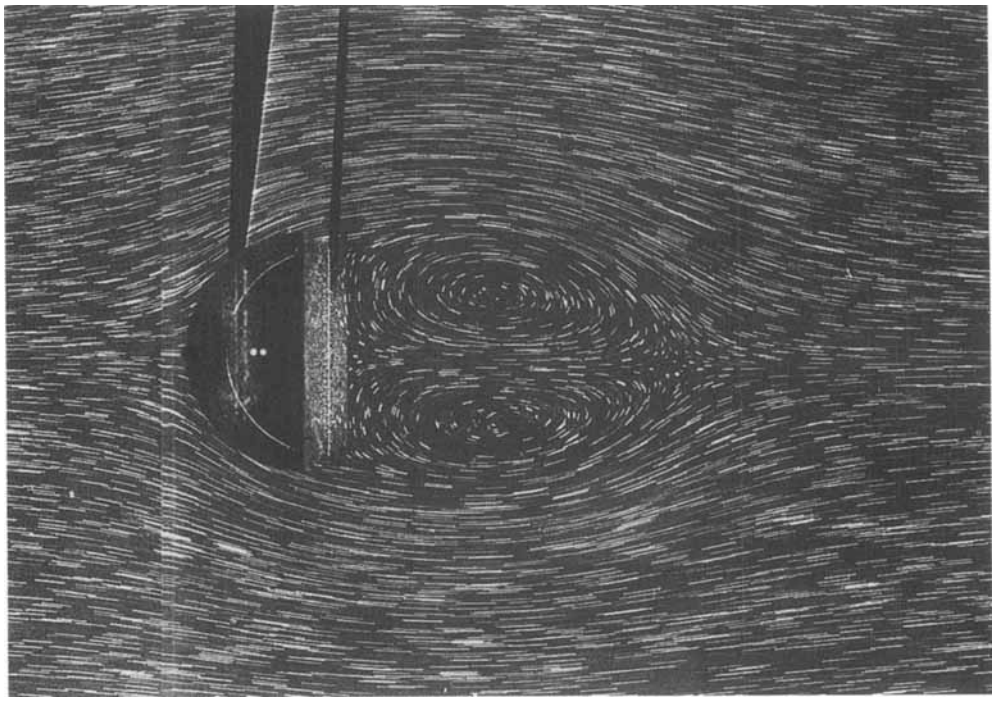

(*b*)

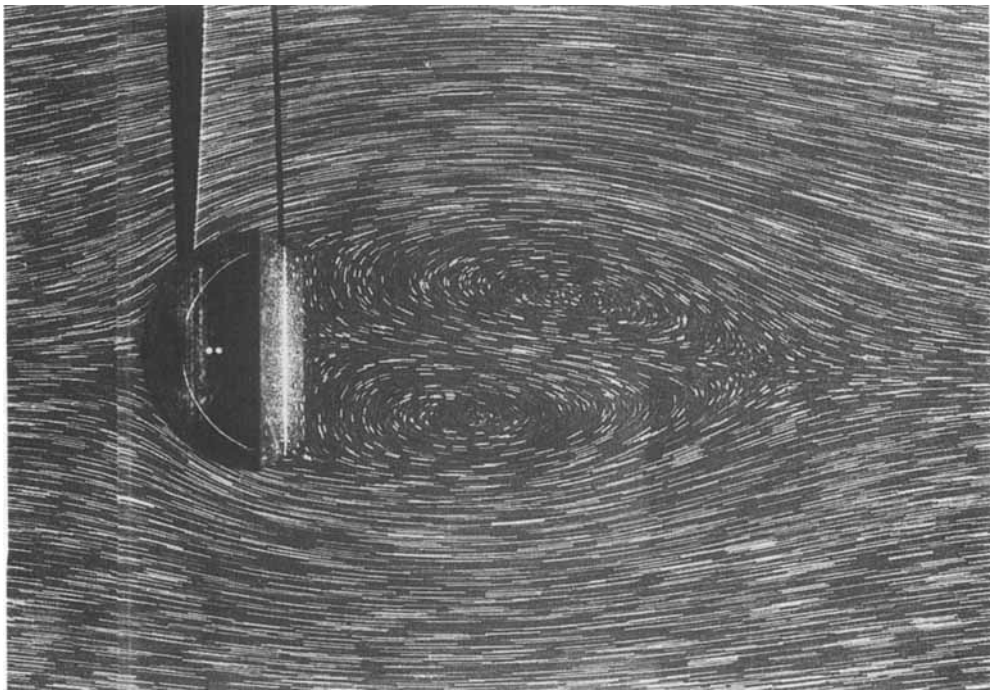

FIGURE 4(*a*, *b*). For caption see page 80.

(*c*)

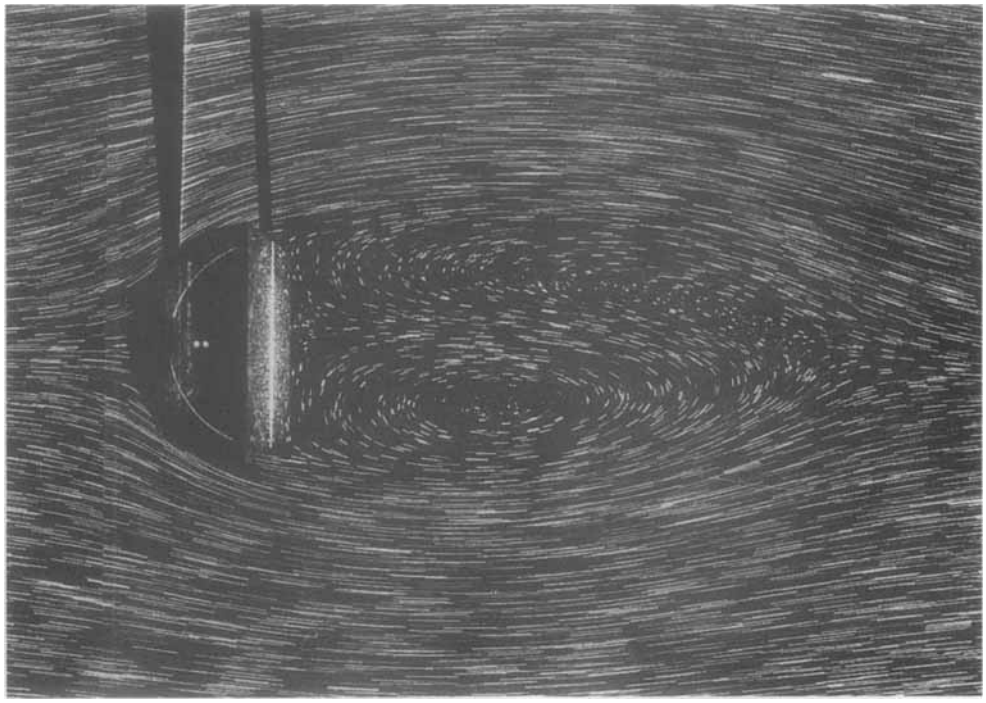

(*d*)

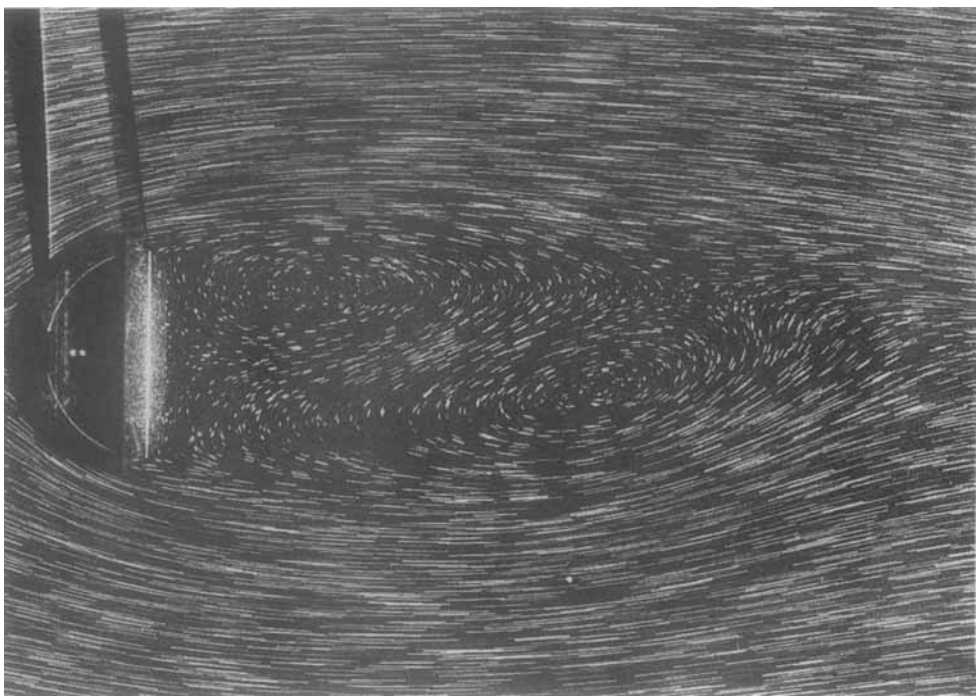

FIGURE 4(*c*, *d*). For caption see page 80.

(*e*)

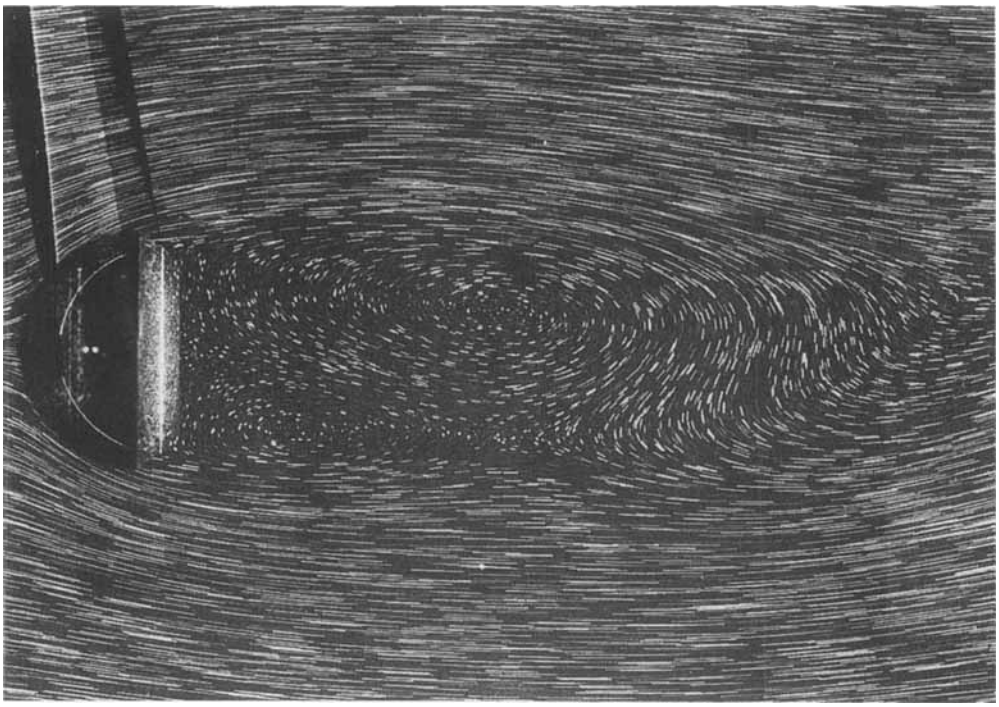

(*f*)

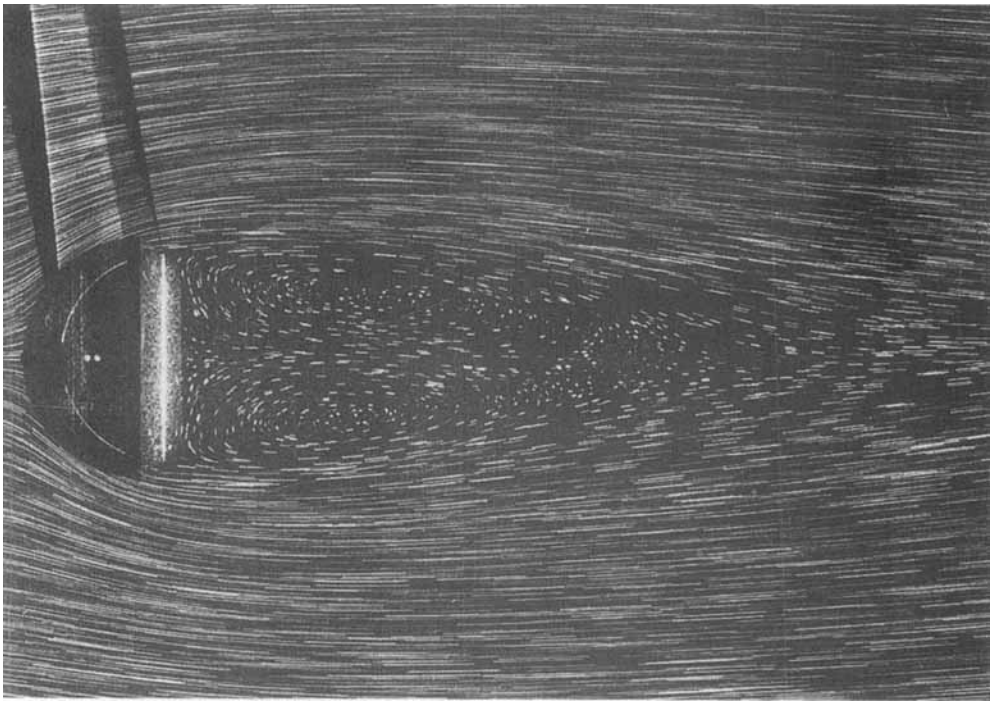

FIGURE 4. Typical stages of the time-development of the wake pattern for the rounded-forebody configuration and the lower-*Re* regime: (*a*)–(*e*) $Re = 100$ and $t^* = 3, 5, 6, 8, 10$; (*f*) $Re = 60$ and $t^* = 10$.

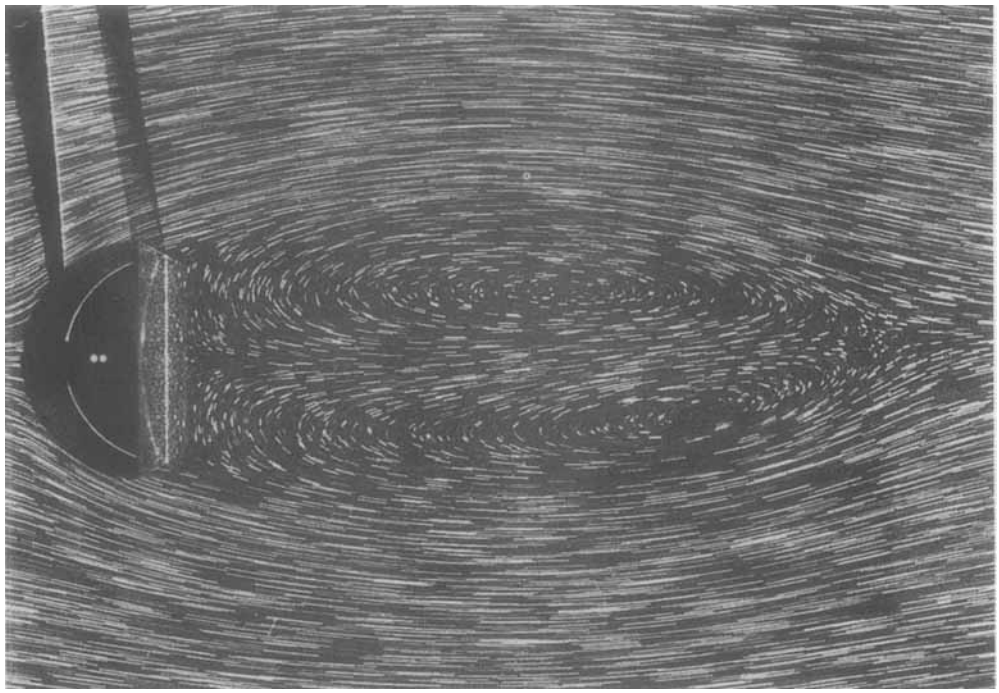

FIGURE 5. Typical wake pattern for the rounded-forebody configuration and transition-Re regime: $Re = 200$, $t^* = 9$.

influence of the body-wall curvature. Thus, a qualitative examination of the two cases is presented in §§ 3 and 4 and a comparative quantitative study in § 5. In order to be able to make this quantitative estimation, the pictures were accurately analysed to deduce the usual geometrical parameters of the R-zone, such as the length L and maximum width l_{max}, the coordinates (x_u, y_u), (x_l, y_l) of the cores of the upper and lower first vortices respectively, as well as their relative angular shift θ. Furthermore, we measured the V_x-component of the velocity along the downstream-axis (cf. figure 3). When the R-zone becomes open, i.e. from the start of the vortex shedding, the free stream penetrates the wake, meandering between the vortices, then, in conformity with the closed-R-zone case, the R-zone length L was taken at the point of the x-axis where $V_x = 0$. The length of the total zone occupied by all the vortices, L', has also been determined to demonstrate the progress of the initial wake perturbation (Boisaubert 1994).

3. Flow-pattern for the rounded-forebody configuration

Let us consider, first, the time-development of the wake in the case where the flat side of the semicircular cylinder is turned downstream and consequently the rounded side faces the oncoming current. A simple qualitative examination of the sequences of pictures, collected for Re regularly ranging between 60 and 600 ($(10 \times 7) \times 2$ pictures, each sequence having been performed twice), shows that the wake structure varies continuously with the increase of Re. Three types of behaviour were distinguished. We will examine the particulars of each of these flow regimes in turn.

(*a*)

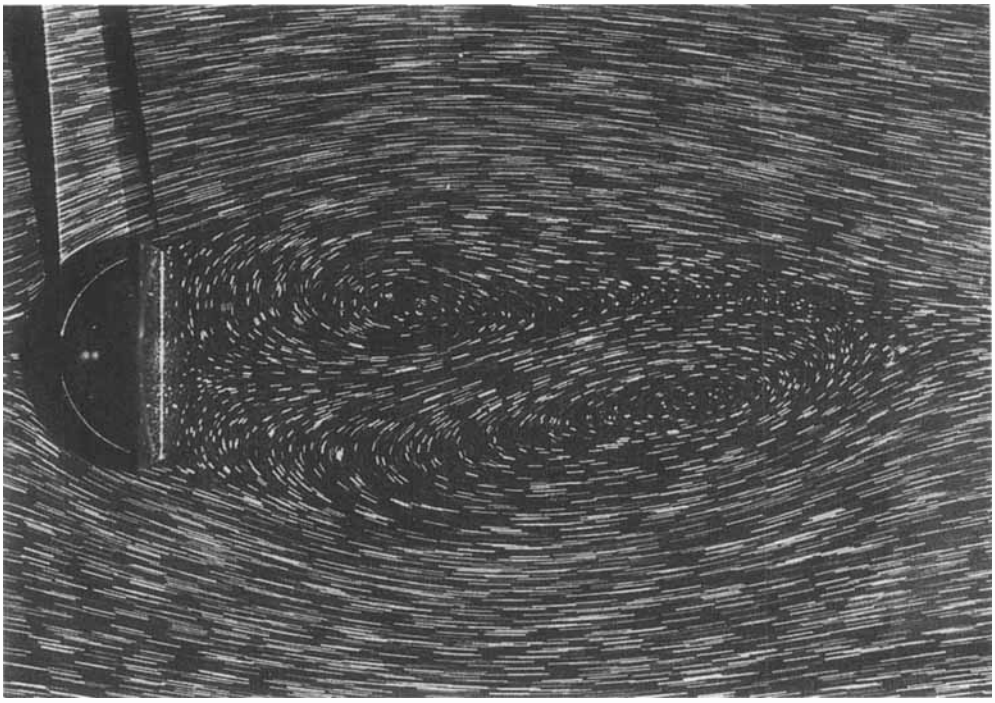

(*b*)

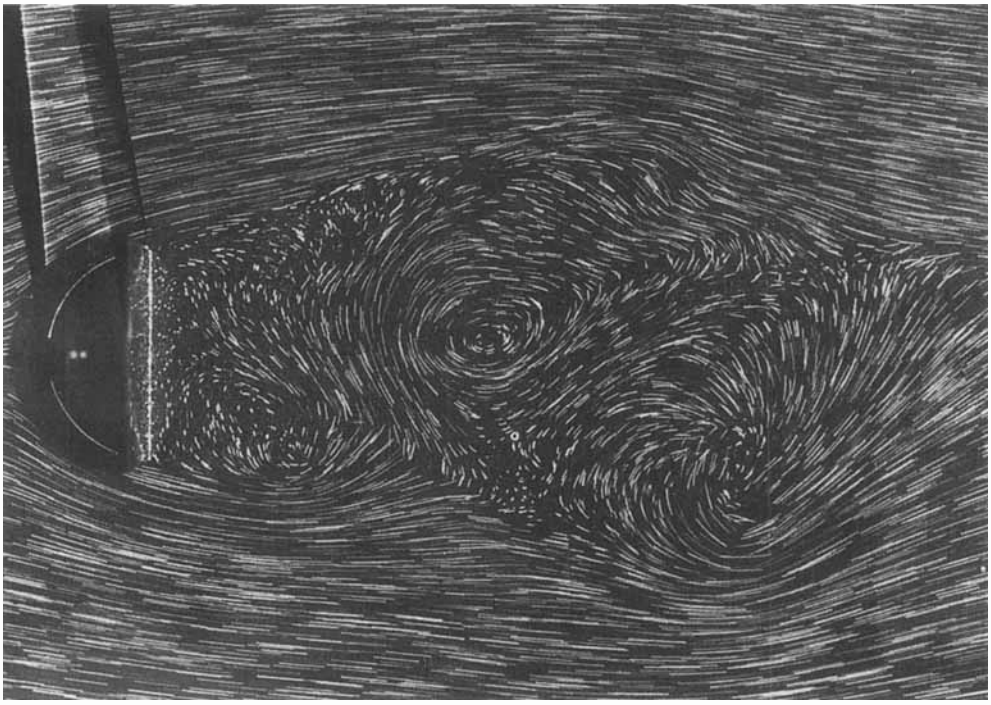

FIGURE 6(*a*, *b*). For caption see facing page.

(*c*)

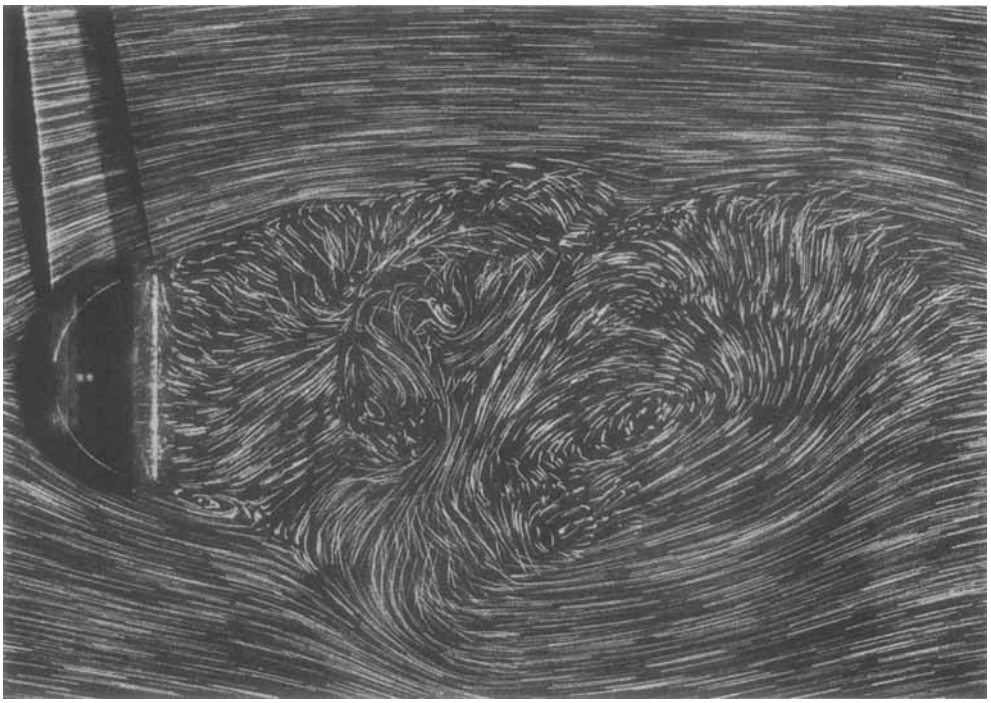

FIGURE 6. Typical wake patterns for the rounded-forebody configuration and higher-*Re* regime: (*a*) $Re = 300$, $t^* = 9$; (*b*) $Re = 400$, $t^* = 10$; (*c*) $Re = 600$, $t^* = 10$.

3.1. *Time-evolution for the lower-Re regime:* $Re = 60$–100

In this regime, the general time-evolution described above, giving rise to an alternate Bénard–von Kármán (B–VK) shedding process, is observed, particularly for $Re = 100$, which constitutes a typical case. However, it is to be remembered that since the camera is moving with the cylinder, the shed vortices do not appear as closed loops. Thus, figure 4 shows successively the symmetrical phase (figure 4*a*), then the start, from $t^* = 4$, of the asymmetry and its development (figure 4*b*), then the shedding of the downstream part of the upper vortex (figure 4*c*), then, from $t^* = 7$, the re-organization of the upstream part of this upper vortex into a new upper vortex and the shedding ($t^* = 8$) of the lower vortex (figure 4*d*), and finally ($t^* = 10$) the simultaneous formation of the second lower vortex and the onset of the shedding of the second upper vortex (figure 4*e*). To sum up, for this rounded-forebody configuration and at $Re = 100$, the following stages in the time-evolution of the wake have been clearly distinguished:

(i) formation of a closed R-zone including symmetrical counter-rotating vortices ($t_s < t^* \leqslant 3$; the initial time t_s of flow separation has not been determined exactly in this experimental study, but it is clearly less than 1);

(ii) onset of asymmetry in a still quasi-attached R-zone ($t^* \approx 4$);

(iii) onset of an alternate B–VK vortex shedding process ($t^* \geqslant 6$).

For $Re = 60$, the same process tends to be established. However, the wake evolves more slowly and the phenomena are not so clearly marked. Thus, the asymmetry appears at $t^* = 5$ instead of 4 and remains very slight, and the splitting of the upper vortex takes place at $t^* = 7$ instead of 6 with only a very small amount being shed.

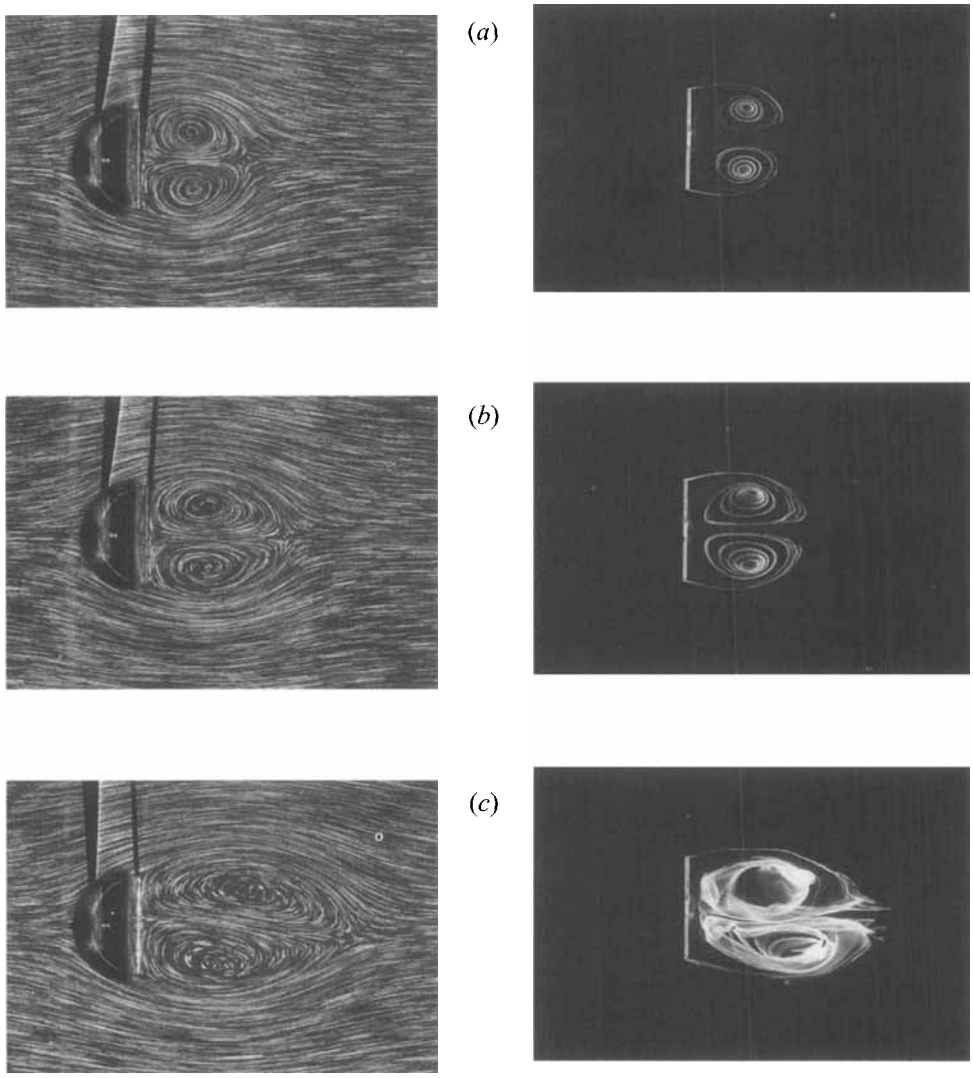

FIGURE 7. Comparative wake development for the rounded-forebody configuration visualized by dispersed and continuous tracers: $Re = 600$, $t^* = 2, 3, 6$ (a–c).

From this stage, the evolution becomes extremely slow with only a very weak splitting of the lower vortex. Consequently, the cores of the two initial vortices remain in a quasi-symmetrical position (see figure 4f for $t^* = 10$). For this Reynolds number, particle-streak visualization is probably not the best method to show the shedding process. Indeed, the velocities are very low at the rear of the R-zone. Note also that the flow has been found extremely sensitive to even very small eventual perturbations (similar to a weak current of convection in the tank) and consequently not exactly reproducible. However, this reproducibility has been well verified in the other cases.

The present vortex-shedding observations are in good agreement with the description by Gerrard (1978), Coutanceau & Defaye (1991) and Green & Gerrard (1993) for the circular cylinder.

(*a*)

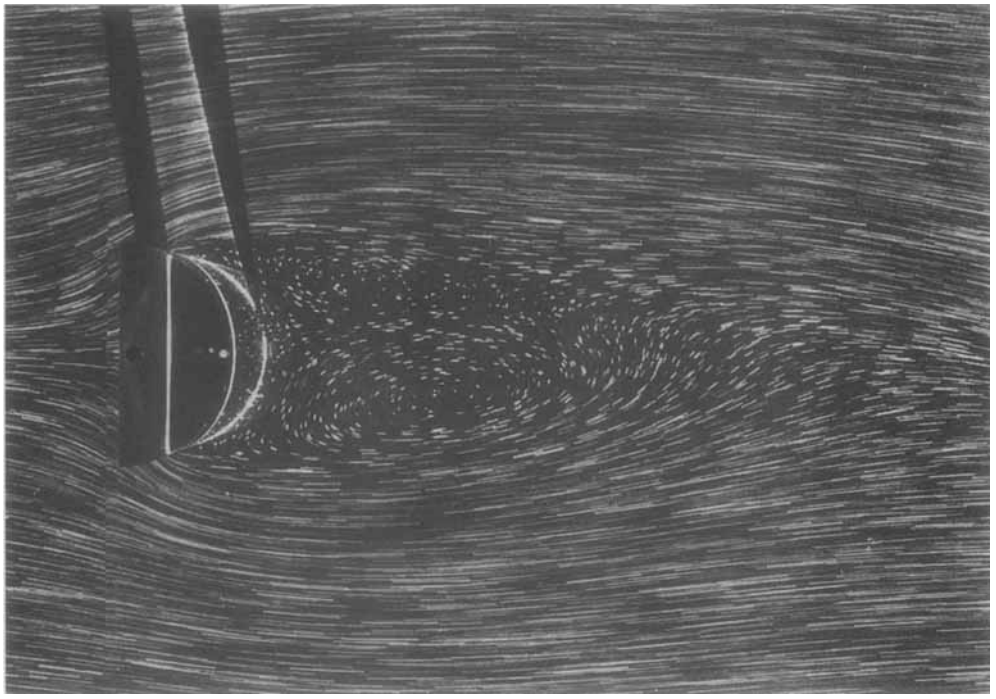

(*b*)

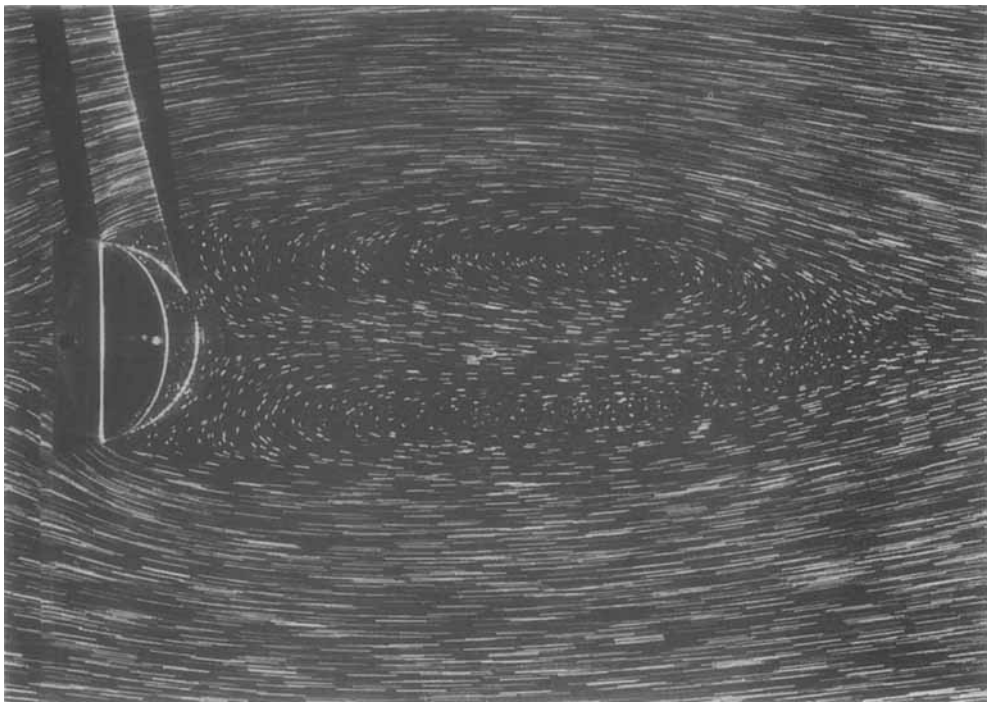

FIGURE 8. Typical wake patterns for the flat-forebody configuration and lower-Re regime: $t^* = 9$ and (*a*) $Re = 60$; (*b*) $Re = 100$.

(*a*)

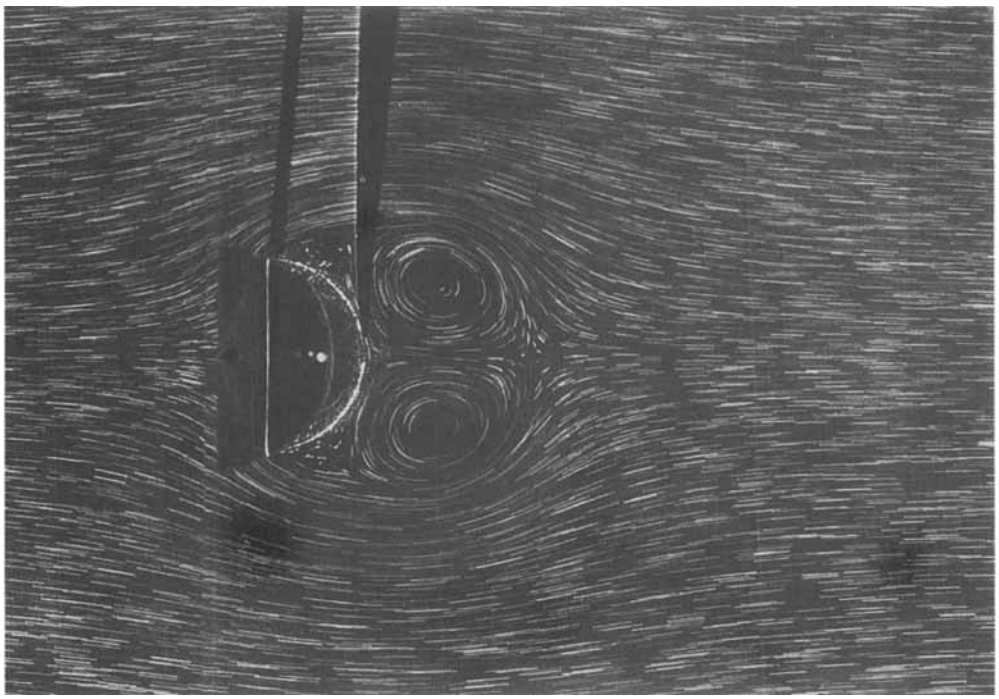

(*b*)

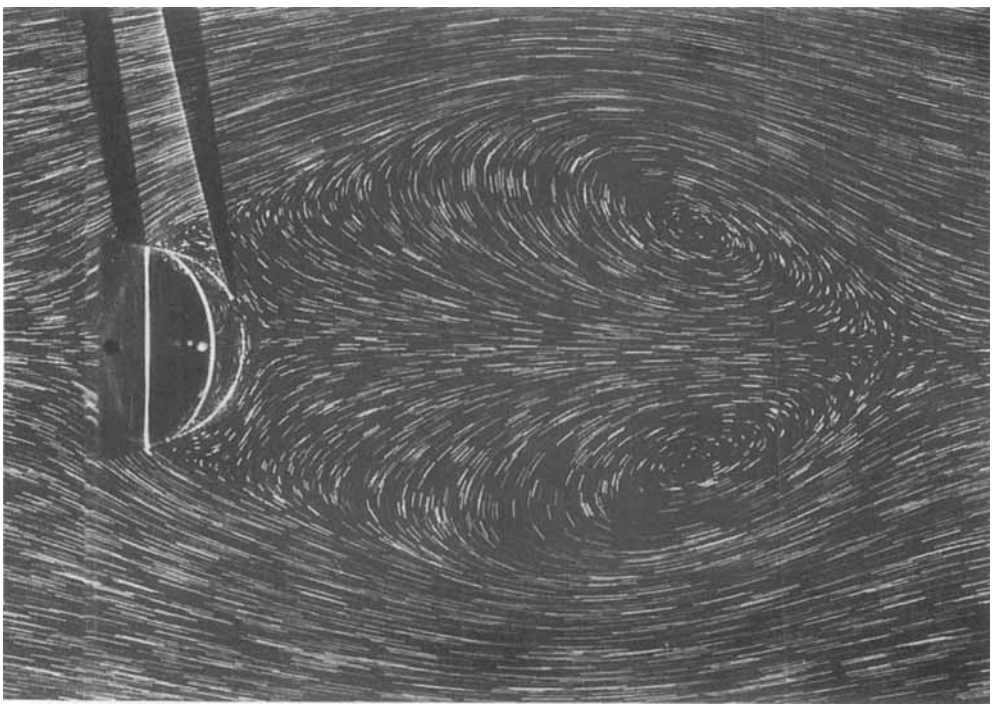

FIGURE 9. Typical wake patterns for the flat-forebody configuration and transition-Re regime: $Re = 200$, and (*a*) $t^* = 2$; (*b*) $t^* = 9$.

3.2. *Time-evolution for the transition-Re regime: Re* ≈ 200

At $Re = 200$, the initial evolution is similar to that described in the previous subsection. Differences in the qualitative behaviour are observable only from $t^* = 4$. Indeed, beyond this time and up to $t^* \approx 6$, the two vortices continue to grow longer quasi-symmetrically, with their cores located about at mid-wake and stretched longitudinally. A relative shifting of one of the vortex cores compared to the other is only detected from $t^* = 7$. But, for this case of $Re = 200$, this core-shifting does not continue to progress beyond $t^* = 8$, because, the other vortex core starts to move in its turn rapidly downstream, giving rise, at $t^* = 9$, to a very long asymmetrical but still quasi-closed R-zone (see figure 5). At the final time, $t^* = 10$, the two vortex cores are clearly shifted to the back of the R-zone with only a small part of the lower vortex (the first one) on the way to being shed. It may be recalled that, at the same time, three vortices were shed for $Re = 100$.

3.3. *Time-evolution for the higher-Re regime*: *Re* = 300–600

Once again, the R-zone remains quasi-closed and symmetrical up to $t^* = 6$, but its length is now clearly shorter, and more so as Re becomes greater. In addition, three-dimensional perturbations occur in the final stage. Thus, once $t^* > 7$, the vortex cores become more and more clearly spiral shaped as Re increases, i.e. from a topological point of view, centres are transformed into foci, because of the occurrence of a local axial core flow as observed, in the case of the circular cylinder, by Pineau *et al.* (1992) and Williamson (1992).

Furthermore, beyond the transition regime, the development with time of the basic vortex-core-shifting phenomenon is again clear (see figure 6*a* for $Re = 300$), progressively inducing again an Re-increasing process of vortex shedding (see figures 6(*b*) and 6(*c*): $Re = 400$ and 600). But, for the greatest Re-value, the vortices which are shed become blurred by the first manifestation of turbulence (figure 6*c*) and the wake flow is clearly three-dimensional (the particle streaks cross the visualized plane).

For $Re = 600$, figure 7 shows, in parallel, the early (up to $t^* = 6$) development of the velocity field and vorticity convection visualized respectively by dispersed solid tracers and by an electrochemical tracer, emitted continuously from a tin wire rolled up around the median section of the body, and washed off from the wall by the current. The progressive appearance of three-dimensional effects in the vortex cores and Kelvin–Helmoltz-type instabilities in the rolled-up separated shear layer (once $t^* = 3$), and then, the onset and the progressive increase of asymmetry and of vortex core blurring are clearly visible in this second set of pictures. Note that this electrochemical visualization has been done only for this greatest Re-value because experiments had to be carried out in water.

4. Details of the flat-forebody-configuration flow pattern

We will now consider the time-evolution of the wake structure when the semicircular cylinder is turned through 180°, i.e. its flat side now faces the oncoming current (flat-forebody configuration); we will make a comparison with the previous case (rounded-forebody configuration). The general principles of the evolution remaining roughly the same, the main object of the present section is to point out the detailed differences in this second arrangement, for the same Re-range: $60 \leqslant Re \leqslant 600$. This should permit us to get an initial evaluation of the respective influence of a flat or rounded side facing the flow. Thus, from a qualitative examination of the numerous

(*a*)

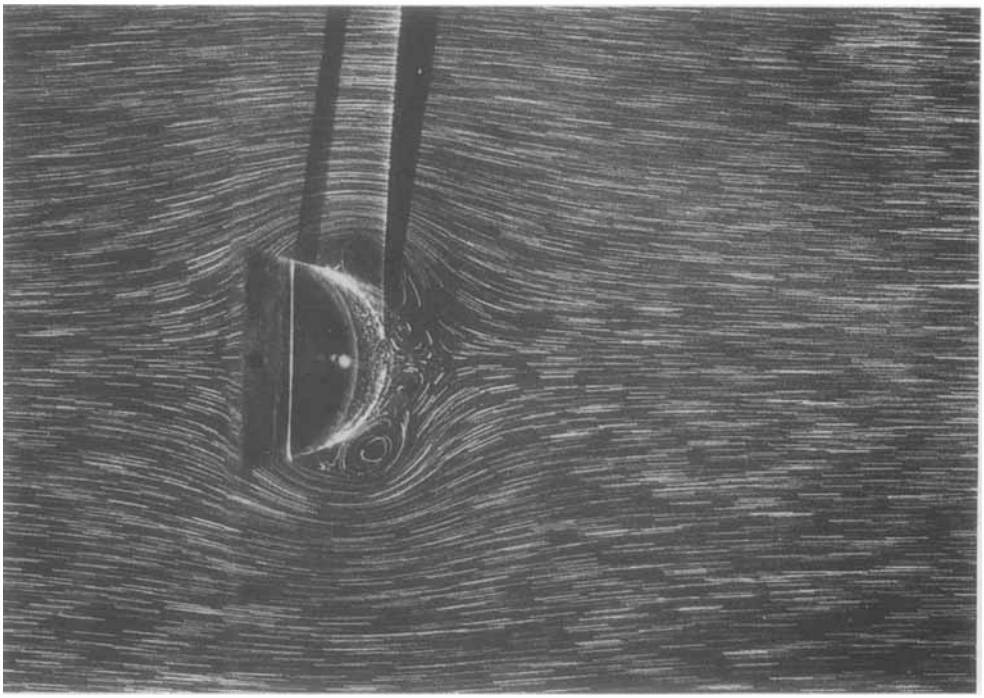

(*b*)

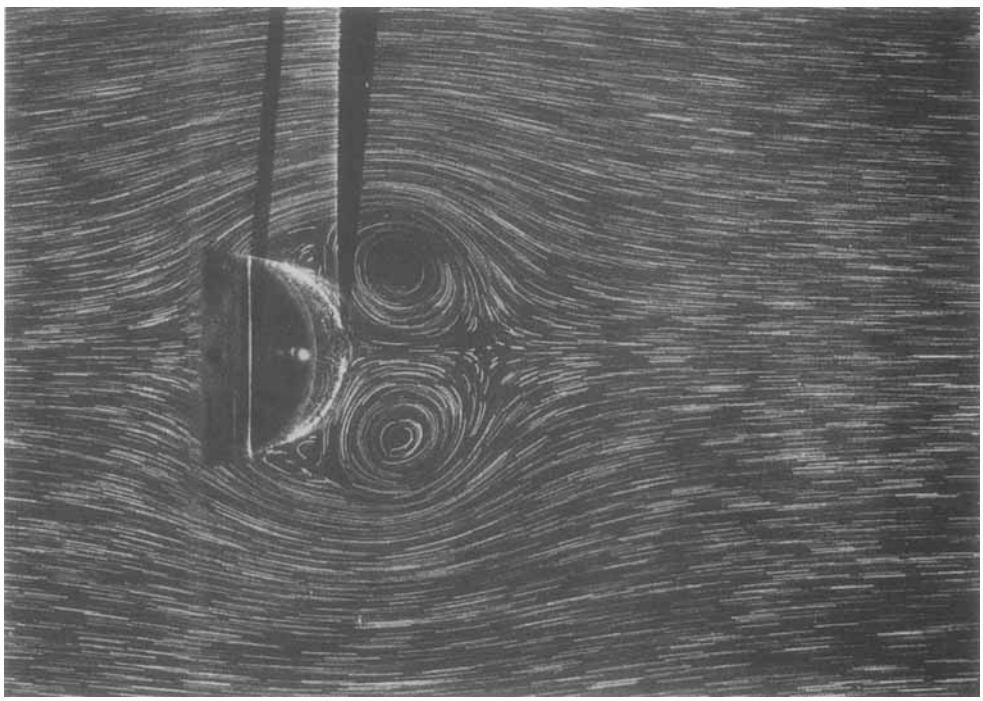

FIGURE 10(*a*, *b*). For caption see facing page.

(*c*)

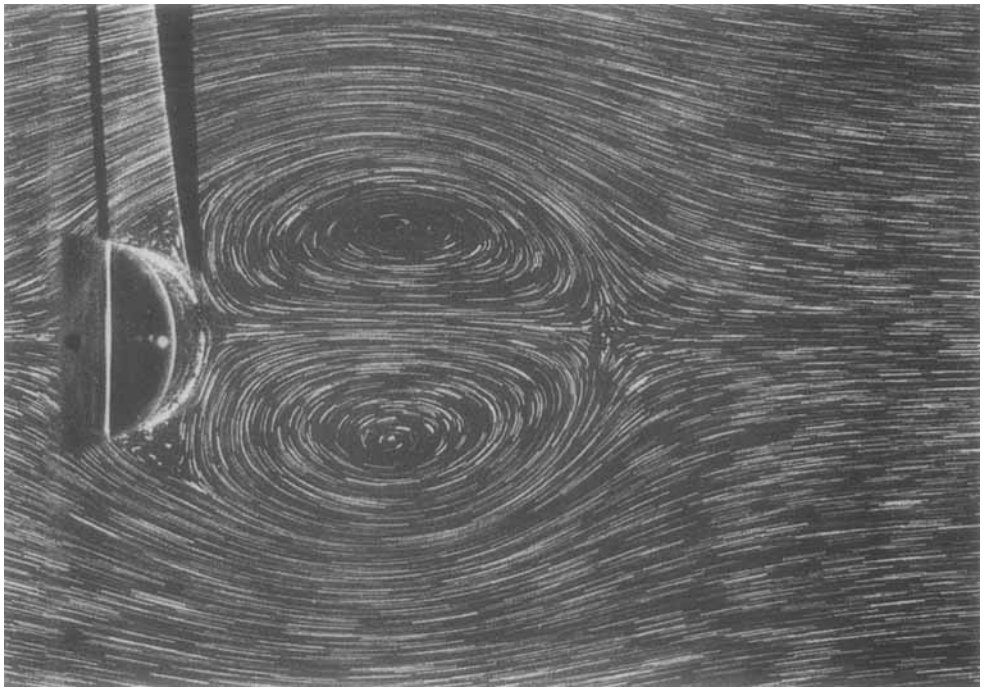

(*d*)

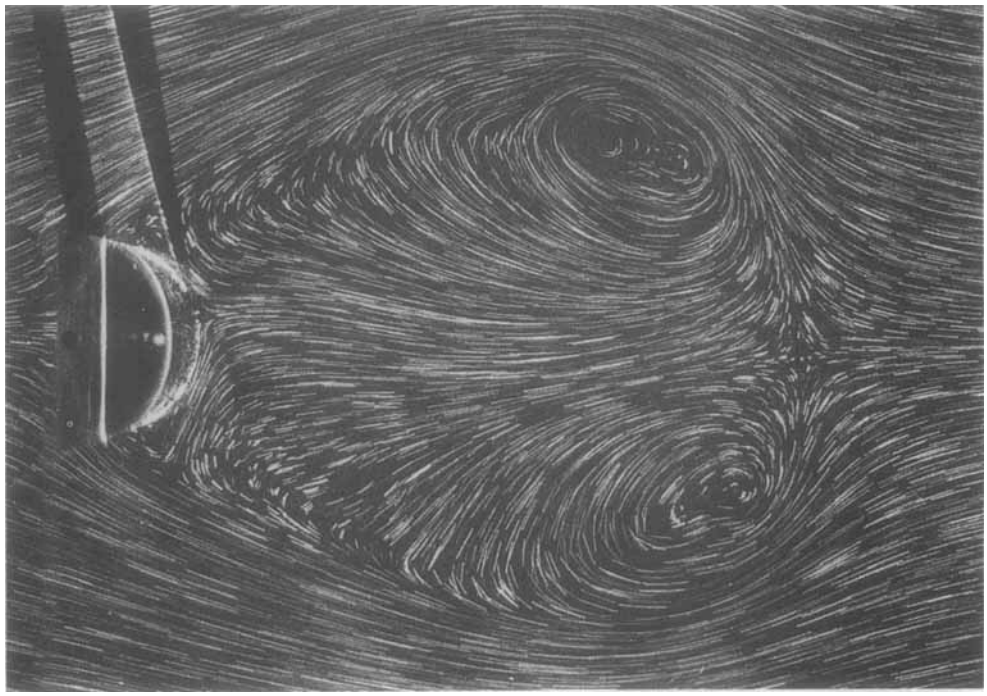

FIGURE 10. Typical stages of the time-development of the wake pattern for the flat-forebody configuration and the higher-Re regime: (*a*)–(*d*) $Re = 500$ and $t^* = 1, 2, 6, 10$.

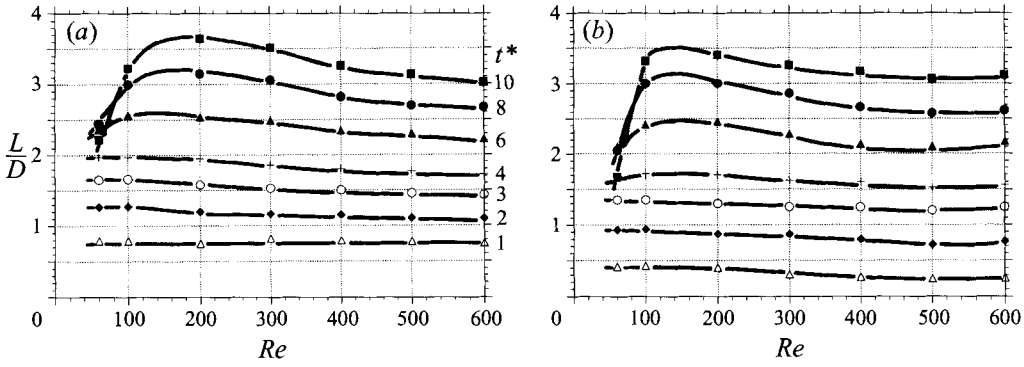

FIGURE 11. R-zone length versus Re for regularly spaced times: (a) rounded-forebody configuration; (b) flat-forebody configuration.

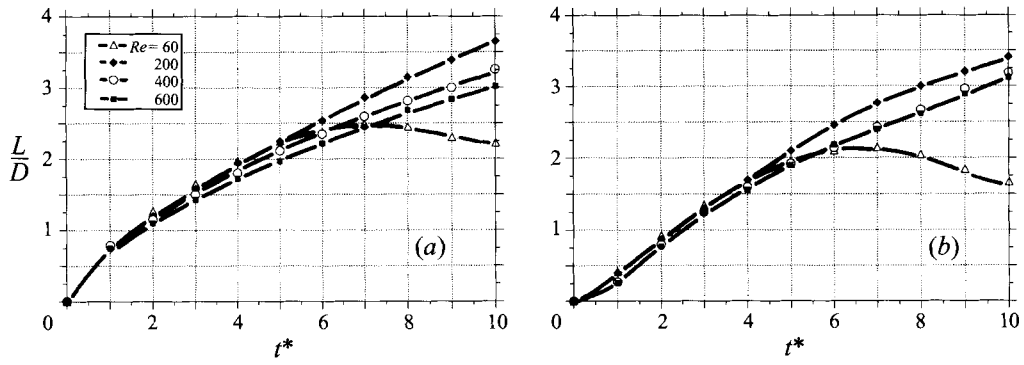

FIGURE 12. Time-development of the R-zone length for selected Re-values: (a) rounded-forebody configuration; (b) flat-forebody configuration.

pictures (once again each time sequence has been repeated to confirm the data), it appears that a change in the Re-evolution of the wake behaviour still occurs in the range $Re \approx 100$–200, with the temporary clear decrease and then annihilation of the B–VK vortex-shedding process. However, with this flat-forebody configuration, shedding annihilation exists up to the final time of observation, i.e. $t^* = 10$, and up to the end of the Re-range studied here, i.e. up to $Re = 600$; the evolution with Re is also more rapid. In fact, up to $Re \approx 200$ analogies in the wake structure are found for the two configurations but for shifted Re-values. Thus, a clear and then a very weak vortex shedding take place respectively at $Re = 60$ (figure 8a) and at $Re = 100$ (figure 8b) like that at $Re = 100$ (figure 4d) and then $Re = 200$ (figure 5) for the first configuration. Furthermore, several typical characteristics appear, more especially in the initial and final phases of the development. Thus, very soon after the impulsive start, the flow separates from the two edges to form a pair of symmetrical contra-rotating vortices. But there, the presence of the rounded afterbody reduces the velocity of the R-zone returning fluid, passing along the body wall, inducing secondary phenomena analogous to those described by Bouard & Coutanceau (1980) for the circular cylinder and confirmed by calculation (initially by Collins & Dennis 1973; Ta Phuoc Loc 1980; Ta Phuoc Loc & Bouard 1985) and experimentally by Honji & Taneda (1969) and Nagata, Nagase & Ito (1989). Thus, with progressively increasing Re, and using the same

terminology as Bouard & Coutanceau (1980), we observe, in each separating R-zone corner, a 'bulge', then an isolated secondary eddy and finally a quasi-pair of secondary eddies (see for example figure 10*b*). Likewise, the 'forewake' phenomenon, with its typical flattened rear, forming in the very early phase of the flow development ($t^* < 2$), is also easily identifiable (see for example figure 10*a*). However, in the present case, all these phenomena appear for smaller Re, being consequently less energetic because the velocities are lower. As examples, the 'bulge' is clearly identified as early as $t^* = 3$ and $Re = 100$, the isolated vortex at $Re = 200$ (see figure 9*a*) and the secondary vortex pair from $Re = 300$–400 instead of about 200, 500 and 1000 respectively for the circular cylinder. Note that, as for the full circular case, these secondary phenomena become more marked and develop more rapidly as Re increases, and decrease with time when the associated main vortex begins to elongate too much downstream (see figure 10*c*), eventually increasing again with the reverse motion of the separation point (Coutanceau *et al.* 1988; Nagata *et al.* 1989). The initial forewake phenomenon becomes clearly visible from $Re = 400$; it causes a clear decrease in the rate of the initial wake development (in both length and velocity), compared to the rounded-forebody configuration. This will be confirmed and evaluated in §4.

On the other hand, in the final stage ($t^* \geqslant 7$) of the time-development, and from $Re = 200$, the R-zone structure takes on a typical shape with the two vortex cores shifted symmetrically at the back of the R-zone and clearly away from the x-axis. This phenomenon, which becomes more marked as Re increases (see figures 9*b* and 10*d*), makes the R-zone of the flat forebody clearly larger at the back than that of the rounded forebody and maintains it quasi-symmetrical up to $t^* = 10$, and up to $Re = 600$. Under these conditions, for this second configuration, the R-zone appears to be composed of two parts, with a quasi-linear increase of its width from the separation points to a maximum value and then a decrease, up to the rear saddle point. The location of the maximum width moves further downstream as Re increases, so that the resulting width decrease is more abrupt as Re becomes higher, making the rear boundary of the R-zone increasingly larger and more flattened (figure 10*d*). For the greatest Re-values (500 and 600) convincing evidence of the clear difference between the wake structures associated with the two body configurations can be found by comparing the pictures of figures 7 and 6(*c*) with those of figure 10.

One may remark that the final structure of the R-zone of the flat forebody is of the same type as that of the normal flat plate found by Taneda & Honji (1971) and Polidori (1994) for $Re \approx 900$ and 1000 respectively. Thus, it appears that the shape of both the forebody and afterbody influences the time-evolution of the corresponding wake.

5. Quantitative comparison

As we have said at the end of §2, the pictures have been analysed in detail to get precise quantitative data for the geometrical R-zone parameters and the velocity distribution along the downstream flow axis. Thus, a large amount of data were collected, pictures for each Re, t^* combination being processed, for each of the two body configurations. Furthermore, the second set of pictures taken for each run, in order to confirm the results, were also used when apparent anomalies were detected. Only some examples could be given in this paper, but other results can be requested from the authors.

Figures 11 to 17 show, in parallel for the two configurations, the respective evolution of the R-zone length L, maximum width l_{max}, some examples of the V_x-velocity-component profiles and the associated maximum $|V_{x_{max}}|$, the vortex-core trajectories

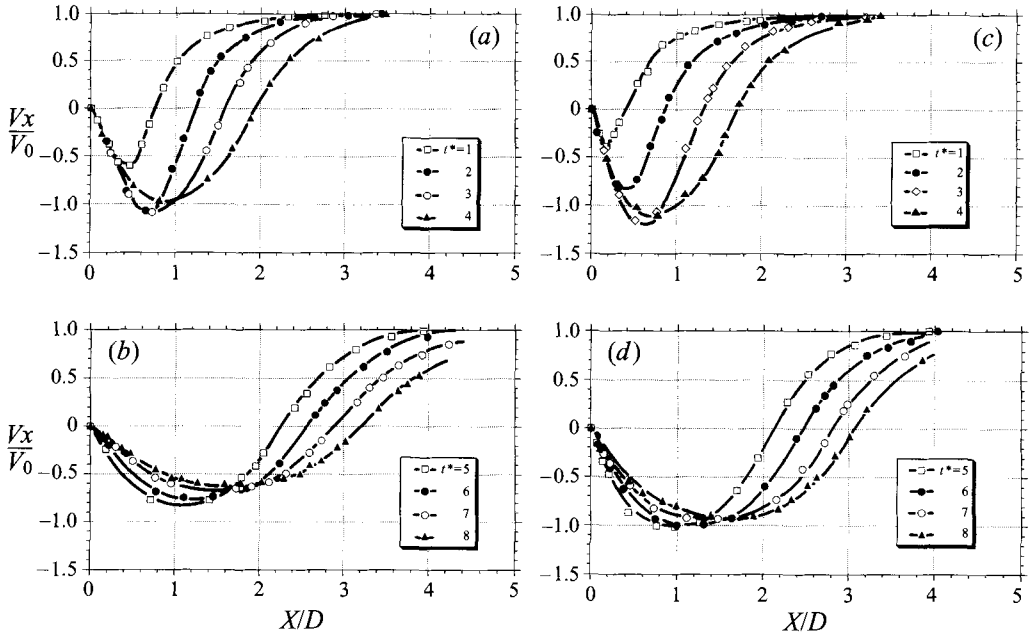

FIGURE 13. Time-evolution of the V_x-velocity component along the flow axis for $Re = 200$ and (a, b) rounded-forebody configuration: (a) $t^* = 1$ to 4; (b) $t^* = 5$ to 8; (c, d) flat-forebody configuration: (c) $t^* = 1$ to 4; (d) $t^* = 5$ to 8.

and the θ-angle between the first two vortices. This parallel presentation permits us to establish a direct comparison. The definitions of the different parameters are given by the schematics of figure 3.

These data confirm and evaluate the behaviour similarities or differences already found from a simple qualitative examination of the pictures. Thus, the change in the wake behaviour as a function of Re is very clear on figures 11(a) and 11(b) which present the R-zone length L for the rounded- and flat-forebody configurations respectively and for times t^* ranging between 0 and 10. It is seen that, as soon as $t^* = t^*_c \approx 6$, L passes through a clear maximum L_{max} for Re somewhat above 100 in the two cases. This passage through a maximum has been considered here as a good manifestation of the wake changeover and has been used to define a critical value Re_c of the Reynolds number. For the flat-forebody configuration, the rate of the initial increase of $L(Re)$ is clearly higher, inducing a sharper maximum, and at a quasi-constant value $Re_c \approx 140$. For the rounded-forebody configuration, on the other hand, the critical Re_c-value evolves, during the same period of time ($6 \leqslant t^* \leqslant 10$, our final time of observation) from 140 to 190. The error on the Re_c-determination is evaluated to be about 5%.

The time-evolution of the R-zone length appears clearer on figure 12(a, b) showing L against t^* for some Re-values. The change in behaviour from $Re = 200$ is well confirmed, as is the clear difference between the two body configurations in the initial rate of increase of L with time.

This R-zone length was determined directly from the pictures, but also in a more accurate manner from the distribution of the V_x-velocity-component along the x-axis: L is the abscissa of zero V_x. Indeed, the returning fluid of the R-zone has a negative V_x-velocity there, whereas it takes a positive value again outside it. As an example, figure 13(a–d) shows these two V_x-curve families for $1 \leqslant t^* \leqslant 8$, at $Re = 200$. The good

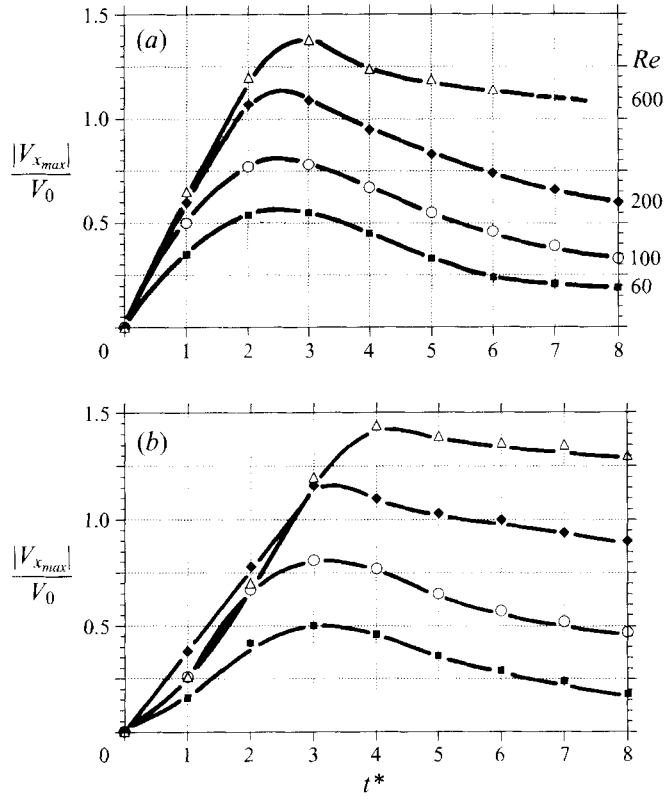

FIGURE 14. Time-evolution of the maximum of the V_x-velocity component inside the recirculating zone for selected Re: (*a*) rounded-forebody configuration; (*b*) flat-forebody configuration.

accuracy of the measurements is well demonstrated by the smoothness of the curves and by their excellent fitting with each other. In addition, the identification of the zone of returning fluid is clear, as well as some typical features such as the maximum of the velocity of the returning flow and the rate of increase of V_x at the R-zone extremity (intersection with the x-axis). These features having been considered as parameters of particular interest to make a quantitative comparison, we have systematically measured these values and plotted their time-evolution as a function of Re. Thus figure 14(*a*, *b*) gives the $|V_{x_{max}}|$-evolutions for the two body configurations. It is seen that $|V_{x_{max}}|$ passes through a maximum for each Re-value. As Re increases from 60 to 600, the magnitude of this maximum $|V_{x_{max}}|_{max}$ evolves from 0.57 to 1.38 and from 0.50 to 1.44 respectively for the rounded and flat forebody; however the time of occurrence of this maximum varies only from about $t^*_{V_{max}} = 2.5$ to 3 and 3 to 4. So this maximum increases clearly with Re, but it is not very sensitive, as neither is its time of occurrence, to the body shape. However, it is clear that the rounded afterbody significantly slows down the initial (especially up to $t^* = 2$) R-zone development both in length and velocity, and more so as Re increases. Thus, for $Re > 200$, the relative drop of the initial part of the $|V_{x_{max}}|$-curves, observed in figure 14(*b*), shows clearly the typical slowing effect induced by the forewake. For the circular cylinder, Bouard & Coutanceau (1980) also found such behaviour, but for $Re > 550$ (see their figure 29). So, it is clear that the presence of the flat forebody promotes this phenomenon. Here, the phenomenon is not found with the flat afterbody, at least up to $Re = 600$. Other striking differences in the two types of R-

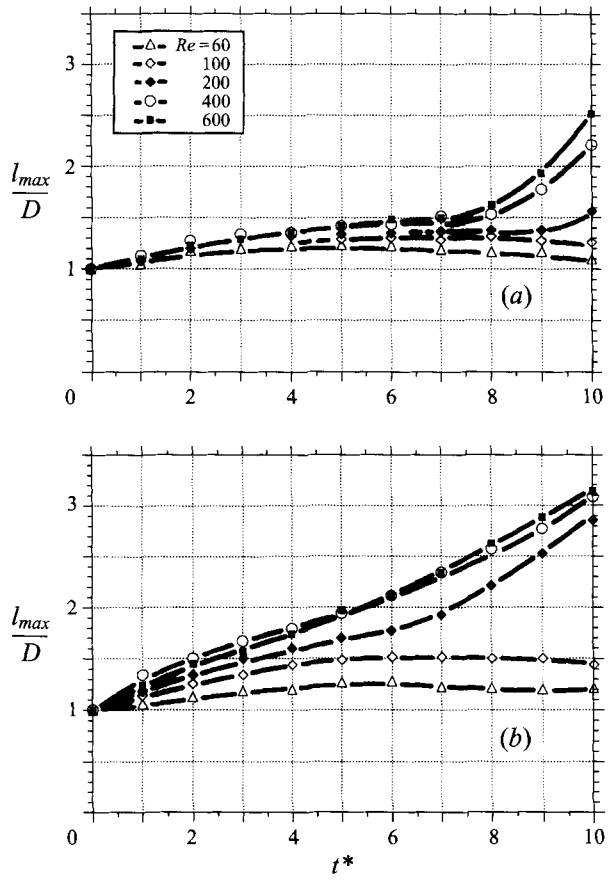

FIGURE 15. Time-evolution of the maximum R-zone width for selected Re-values: (*a*) rounded-forebody configuration; (*b*) flat-forebody configuration.

zone structure evolutions associated with the two body configurations appear when comparing the curves of figures 15(*a*, *b*), 16(*a*–*c*) and 17(*a*–*c*) which show in parallel the time-evolution of the maximum width l_{max}, the trajectories of the vortex cores†, and their angular shift θ for Re-values distributed on each side of the critical transition Reynolds number Re_c for which a change in the flow regime has been observed, namely $100 < Re_c < 200$. In the l_{max}-curves, this change in the flow regime is particularly well shown, especially for the flat forebody with a continuous rapid increase, beyond $t^* = 5$ or 6, of the R-zone width from $Re = 200$, instead of a quasi-stagnation or even a slight decrease for Re up to 100. This is confirmed by the vortex-core trajectories (figure 16). The θ-curves permit a comparison of the vortex-shedding activity: a clear oscillation of the θ-curves indicates the effectiveness of the vortex-shedding process,but a slight oscillation indicates only a fairly small initial instability. During the period of time for which the R-zone remains symmetrical, θ is zero.

† Note that, the flow being unsteady, the vortex cores located on the particle-streak visualization pictures in the present analysis do not correspond generally to the vorticity maxima and are dependent on the frame of observation; taking into account that the pictures have been taken in a frame fixed to the body, this later property becomes sensitive as soon as the vortices start to move downstream (see Coutanceau & Ménard 1985 and Chen, Ou & Pearlstein 1993).

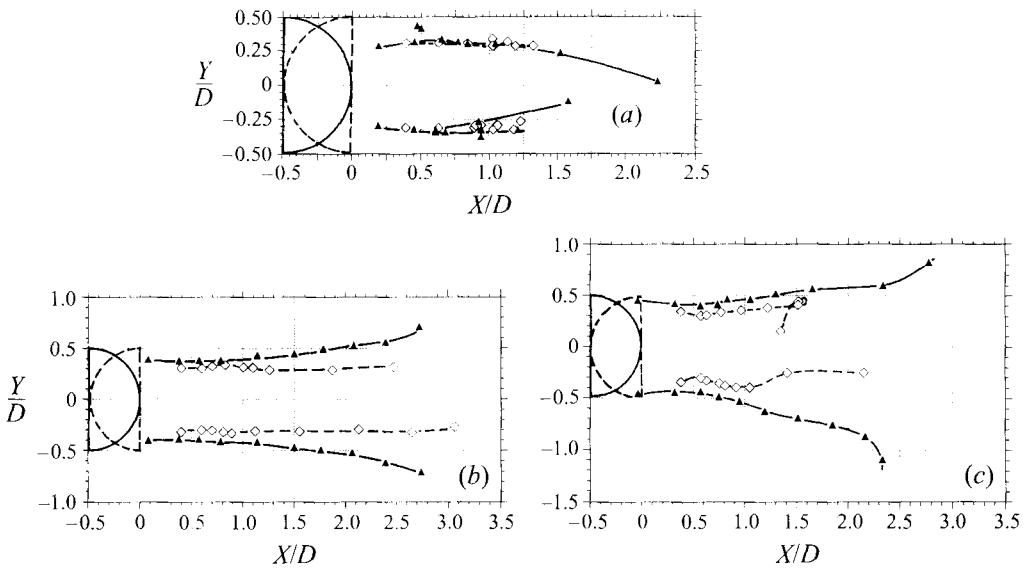

FIGURE 16. Comparative vortex-core trajectories for the rounded-forebody (◇) and flat-forebody (▲) configurations: (*a*) $Re = 60$; (*b*) $Re = 200$; (*c*) $Re = 600$.

6. Conclusions

Numerous original data have been obtained in the present work, studying the comparative early formation of the near wake behind a short ($A = 5.20$) semicircular-section cylinder when its position relative to the free stream is reversed, the Reynolds number being in a sensitive and interesting domain, i.e. 60–600. From these two shape configurations, new insight into the relative effect of the rounded/flat fore-/after-body has been deduced showing the analogies and differences in the near-wake behaviour.

Thus, for the two shape configurations, a clear change in the time-development has been shown, beyond the first phase necessary for the B–VK vortex-shedding process to take place ($t^* \geqslant 6$), when the Reynolds number exceeds a critical value Re_c. It appears that Re_c increases with time for the rounded-forebody configuration, whereas it takes a quasi-constant value for the flat-forebody one and even tends to slightly decrease. The final Re_c-value ($Re_c(t^* = 10)$) is quite sensitive to the body shape. Thus, defined from the maximum of the $L(Re)$-curves, these final values of Re_c are found to be, within about 5%, 190 and 140 for the first and second configuration respectively. Furthermore, the importance of the changeover in the wake structure itself appears clearly influenced by the wall curvature. Thus, it has been shown that for $Re > Re_c$, the flat forebody induces a clear shifting of the vortex cores to the back of the recirculating zone and away from the flow axis, causing a clear enlargement of its downstream part and preventing the onset of the process of vortex shedding by keeping it in a quasi-symmetrical configuration. On the other hand, the associated rounded afterbody induces, from $Re \approx 200$, secondary separations and vortices and consequently induces two phases in the rate of the time-development of the near wake. The primary phase, often called the forewake according to Bouard & Coutanceau (1980), corresponds to an initial (up to about $t^* = 1.5$) low evolution of the recirculating zone, both in velocity and length, exhibiting a particular flattened shape. These phenomena appear to be promoted by the flat front side which has fixed separating points and so occur for lower Reynolds numbers than for the full circular cylinder. Other quantitative evaluations of

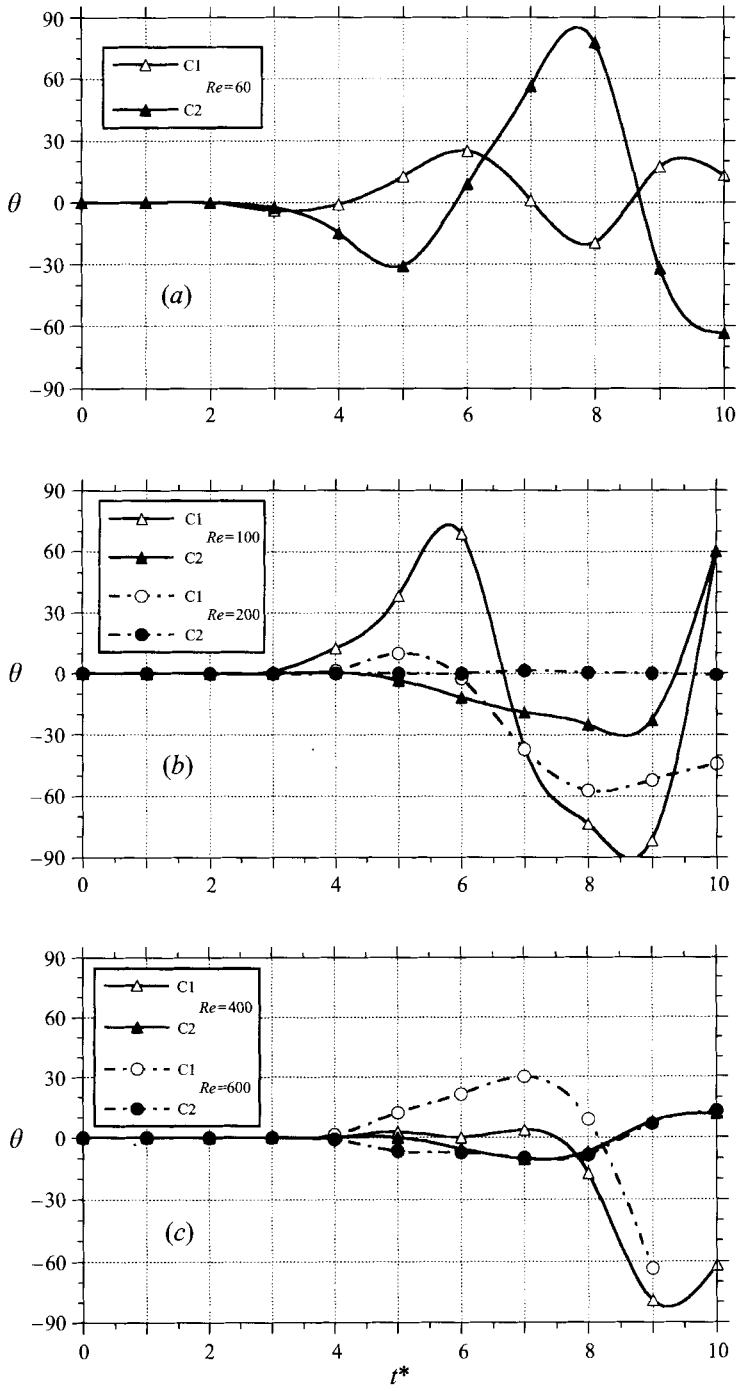

FIGURE 17. Comparative time-evolution of the relative angular shift θ between the two initial vortex cores for the rounded-(C1) and flat-(C2) forebody configurations: (*a*) $Re = 60$; (*b*) $Re = 100$–200; (*c*) $Re = 400$–600.

the observed differences are deducable from the plots included in the present paper or may be requested from the authors.

Based upon this particularly simple and striking example of change in geometrical configuration, the present findings are concerned with the initial period of the flow development. However, it is recognized that this initial flow behaviour conditions the subsequent evolution and gives a first idea of what will happen in the quasi-established situation and consequently is useful for both theoretical developments and industrial applications.

Further studies, considering other typical shapes (see §1), which are now being performed (Ehrmann 1996), will complete these first sets of data and will permit us to deduce more clearly the respective influence of the fore- and afterbody shape by varying only one of the two sides, in contrast to the present analysis where the shapes of the two sides were changed simultaneously. Spanwise visualizations are also being undertaken to uncover the role of the endplates on the observed phenomena. Indeed, some previous studies have shown a possible clear interaction in the *Re*-range considered here (Slaouti & Gerrard 1981; Gerich & Eckelmann 1982; Williamson 1988, 1989; Pineau *et al.* 1992; Ehrmann, Boisaubert & Coutanceau 1994).

But, the present data already show that the two final Re_c-values that we have deduced from the present starting flow experiments, namely 190 and 140 for the first and second configuration respectively, are similar to the critical Reynolds number for transition, of between 170 and 189 (the more recent value), at which the fully developed circular-cylinder wake has been found by numerical simulations to become unstable to spanwise perturbations, so becoming intrinsically three-dimensional (Karniadakis & Triantafyllou 1992; Noak & Eckelmann 1994; Barkley & Henderson 1996; Henderson & Barkley 1996), and to the experimental Re_c-value of 194 given by Williamson (1996) as the upper limit of the laminar shedding range.

So it might be that the changeover, observed here in the second phase of the *Re*-wake development for each of the two configurations, is associated with the onset of a secondary instability of the primary vortex shedding. This would prove that, past t_c^*, the initial flow already contains its three-dimensional unstable character. Here the spanwise instability is probably triggered by the perturbation induced by the endplates and develops with time differently according to the body shape.

Very recently this has been confirmed, especially with the downstream hollow-face semicircular shell, one of the particular nominally two-dimensional bodies we considered recently (Ehrmann 1996).

A three-dimensional numerical simulation, focused on the respective influence of the body cross-section shape and of endplates on the developing wake of a short circular cylinder would be also of great interest in providing complementary insights into this fundamental and also practical problem and to compare with the present results.

The authors are very much indebted to Professors S. C. R. Dennis and J. R. Defaye for their help in improving their English texts and to the referees for their valuable remarks.

REFERENCES

ABED-MERAÏM, K. 1992 Etude expérimentale de l'écoulement plan engendré par la translation d'une coque semi-circulaire pour des nombres de Reynolds allant de 0 à 40. Thèse de l'Université de Poitiers.

BARKLEY, D. & HENDERSON, R. D. 1996 Three-dimensional Floquet stability analysis of the wake of a circular cylinder. *J. Fluid Mech.* (to appear).

BOISAUBERT, N. 1994 Particularités du sillage à l'aval d'un cylindre semi-circulaire, face plane amont ou aval. *Rapport de D.E.A. de l'Université de Poitiers.*

BOUARD, R. & COUTANCEAU, M. 1980 The early stage of development of the wake behind an impulsively started cylinder for $40 < Re < 10^4$. *J. Fluid Mech.* **101**, 583–607.

CHEN, Y. M., OU, Y. R. & PEARLSTEIN, A. J. 1993 Development of the wake behind a circular cylinder impulsively started into rotatory and rectilinear motion. *J. Fluid Mech.* **253**, 449–484.

COLLINS, W. M. & DENNIS, S. C. R. 1973 Flow past an impulsively started circular cylinder. *J. Fluid Mech.* **60**, 105–127.

COUTANCEAU, M. & BOUARD, R. 1977*a* Experimental determination of the main features of the viscous flow in the wake of a circular cylinder in uniform translation. Part 1. Steady flow. *J. Fluid Mech.* **79**, 231–256.

COUTANCEAU, M. & BOUARD, R. 1977*b* Experimental determination of the main features of the viscous flow in the wake of a circular cylinder in uniform translation. Part 2. Unsteady flow. *J. Fluid Mech.* **79**, 257–272.

COUTANCEAU, M., BOYCE, P. & GUÉRINEAU, G. 1988 Sur le rôle des décollements d'ordre supérieur sur la naissance de l'instabilité secondaire de la frontière d'un cylindre circulaire. *C. R. Acad. Sci. Paris* (II) **306**, 1259–1263.

COUTANCEAU, M. & DEFAYE, J. R. 1991 Circular cylinder wake configurations: a flow visualization survey. *Appl. Mech. Rev.* **44**, 255–305.

COUTANCEAU, M. & MÉNARD, C. 1985 Influence of rotation on the near-wake development behind an impulsively started circular cylinder. *J. Fluid Mech.* **158**, 399–446.

DENNIS, S. C. R., WANG QIANG, COUTANCEAU, M. & LAUNAY, J. L. 1993 Viscous flow normal to a flat plate at moderate Reynolds numbers. *J. Fluid Mech.* **248**, 605–635.

EHRMANN, P. 1996 Etude comparative de la formation des sillages en fonction de la forme des obstacles. Application à la coque semi-circulaire. Thèse de l'Université de Poitiers.

EHRMANN, P., BOISAUBERT, N. & COUTANCEAU, M. 1994 Development of Taylor–Görtler vortices in the near wake of a nominally semi-circular shell. *Bull. Am. Phys. Soc.* **39**, 1948–1949.

GERICH, D. & ECKELMANN, H. 1982 Influence of end-plates and free ends on the shedding frequency of circular cylinders. *J. Fluid Mech.* **122**, 109–121.

GERRARD, J. H. 1978 The wakes of cylindrical bluff bodies at low Reynolds numbers. *Phil. Trans. R. Soc. Lond.* A **288**, 351–382.

GREEN, R. B. & GERRARD, J. H. 1993 Vorticity measurements in the near wake of a circular cylinder at low Reynolds numbers. *J. Fluid Mech.* **246**, 675–691.

HENDERSON, R. D. & BARKLEY, D. 1996 Secondary instability in the wake of a circular cylinder. *Phys. Fluids* (to appear).

HONJI, H. & TANEDA, S. 1969 Unsteady flow past a circular cylinder. *J. Phys. Soc. Japan* **27**, 1668–1677.

KALRA, T. R. & UHLHERR, P. H. T. 1973 Geometry of bluff body wakes. *Can. J. Chem. Engng* **51**, 655–658.

KARNIADAKIS, G. E. & TRIANTAFYLLOU, G. S. 1992 Three-dimensional dynamics and transition to turbulence in the wake of bluff objects. *J. Fluid Mech.* **238**, 1–30.

NAGATA, H., NAGASE, I. & ITO, K. 1989 Unsteady flows past a circular cylinder started impulsively in the Reynolds number range $500 < \mathrm{Re} < 10^4$. *JSME Intl J.* (II) **32**, 540–549.

NOACK, B. R. & ECKELMANN, H. 1994 A global stability analysis of the steady and periodic cylinder wake. *J. Fluid Mech.* **270**, 297–330.

PINEAU, G., TEXIER, A., COUTANCEAU, M. & TA PHUOC LOC 1992 Experimental and numerical visualization of the 3D-flow around a short circular cylinder fitted with end-plates. In *Flow Visualization VI* (ed. Y. Tanida & H. Miyashiro), pp. 343–347. Springer.

POLIDORI, G. 1994 Etude par visualisation de sillages tridimensionnels. Application à un profil rectangulaire. Thèse de l'Université de Poitiers.

POLIDORI, G., PINEAU, G., ABED MERAÏM, K. & COUTANCEAU, M. 1992 Shedding process of the initial vortices from impulsively started cylinders at $Re = 1000$: end and body geometry effects. In

Bluff-Body Wakes, Dynamics and Instabilities (ed. H. Eckelmann, J. M. R. Graham, P. Huerre & P. A. Monkewitz), pp. 285–288. Springer.

SLAOUTI, A. & GERRARD, J. H. 1981 An experimental investigation of the end effects on the wake of a circular cylinder towed through water at low Reynolds numbers. *J. Fluid Mech.* **112**, 297–314.

TANEDA, S. & HONJI, H. 1971 Unsteady flow past a flat plate normal to the direction of motion. *J. Phys. Soc. Japan* **30**, 262–272.

TA PHUOC LOC 1980 Numerical analysis of unsteady secondary vortices generated by an impulsively started circular cylinder. *J. Fluid Mech.* **100**, 111–128.

TA PHUOC LOC & BOUARD, R. 1985 Numerical solution of the early stage of the unsteady viscous flow around a circular cylinder: a comparison with experimental visualization and measurements. *J. Fluid Mech.* **160**, 93–117.

WILLIAMSON, C. H. K. 1988 The existence of two stages in the transition to three-dimensionality of a cylinder wake. *Phys. Fluids* **31**, 3165–3168.

WILLIAMSON, C. H. K. 1989 Oblique and parallel modes of vortex shedding in the wake of a circular cylinder at low Reynolds numbers. *J. Fluid Mech.* **206**, 579–627.

WILLIAMSON, C. H. K. 1992 The natural and forced formation of spot-like 'vortex dislocations' in the transition of a wake. *J. Fluid Mech.* **243**, 393–441.

WILLIAMSON, C. H. K. 1996 Vortex dynamics in the cylinder wake. *Ann. Rev. Fluid Mech.* **28**, 477–539.

WILLIAMSON, C. H. K. 1996 Mode A secondary instability in wake transition. *Phys. Fluids* **8**, 1680–1682.

WILLIAMSON, C. H. K. & PRASAD, A. 1993 A new mechanism for oblique wave resonance in the 'natural' far wake. *J. Fluid Mech.* **256**, 269–313.